Photonic–plasmonic-coupled nanoantennas for polarization-controlled multispectral nanofocusing

J. Trevino,[1] G. F. Walsh,[2,3] E. F. Pecora,[2] S. V. Boriskina,[4] and L. Dal Negro[1,2,*]

[1]*Division of Materials Science and Engineering, Boston University, 15 Saint Mary's Street, Brookline, Massachusetts 02446, USA*

[2]*Department of Electrical and Computer Engineering & the Photonics Center, 8 Saint Mary's Street, Boston, Massachusetts 02215, USA*

[3]*U.S. Army Natick Soldier Research Development and Engineering Center, 15 Kansas Street, Natick, Massachusetts 01760, USA*

[4]*Department of Mechanical Engineering, Massachusetts Institute of Technology, 77 Massachusetts Ave., Cambridge, Massachusetts 02139, USA*

**Corresponding author: dalnegro@bu.edu*

Received August 16, 2013; accepted September 13, 2013;
posted October 17, 2013 (Doc. ID 195959); published November 14, 2013

We report on the design and experimental demonstration of array-enhanced nanoantennas for polarization-controlled multispectral nanofocusing in the near-IR spectral range. We design plasmonic double bow-tie nanoantennas-coupled to multiple-periodic nanoparticle arrays to harvest radiation of designed wavelengths from a large spatial area and to focus it into a targeted nanoscale region. Near-field calculations were performed on a gold nanoantenna array using three-dimensional finite difference time domain simulations. Cross-shaped optical nanoantennas were fabricated on glass substrates using electron beam lithography. The optical characterization of the fabricated nanoantennas was performed using second harmonic excitation spectroscopy that demonstrates multiwavelength photonic coupling in good agreement with the antenna modeling. The nanoantenna structures introduced in this Letter provide the ability to focus optical energy into deep subwavelength areas and to address multiple spectral regions with polarization control. Such attributes are highly desirable in optical biosensing, enhanced Raman scattering, and for nonlinear plasmonic applications.

OCIS codes: (240.5440) Polarization-selective devices; (250.5403) Plasmonics; (350.4238) Nanophotonics and photonic crystals.

http://dx.doi.org/10.1364/OL.38.004861

Plasmonics, which aims at the manipulation of surface charge density oscillations of free electrons in metals (termed surface plasmons) and at their efficient conversion to propagating photons, has become a mature technology for nanoimaging and bio(chemical) sensing and holds high promise for implementation of chip-scale information processing networks [1]. Recently, plasmonic nanoantennas have been shown to concentrate incident light to length scales much smaller than the diffraction limit at optical frequencies [2]. Optical nanoantennas have recently been utilized for the enhancement of molecular fluorescence [3], nonlinear optical processes [4,5], optical biosensing [6,7], and photovoltaics [8]. In this Letter, we design and demonstrate a polarization-controlled photonic–plasmonic nanoantenna array that concentrates near-IR radiation to a single subwavelength spot at multiple wavelengths. The design concept builds on the previous work by Boriskina and Dal Negro [9], where multiple-periodic plasmon grating structures were shown to efficiently funnel optical radiation into a nanoparticle dimer by the coherent radiative coupling provided by surrounding metallic nanospheres. In this configuration, the resonant wavelength of the antenna can be switched between two well-defined spectral locations by the polarization state of the incident light. This type of device has the potential to be used for multiplexed nonlinear sensing, near-field imaging, and to resonantly enhance both the pumping and the emission efficiency of sources (e.g., fluorescence, Raman, broadband nonlinear processes).

In this Letter, we independently designed two different periodic chains of gold (Au) nanocylinders to diffractively couple the incident field into a centrally located double bow-tie antenna (DBA), as shown in Figs. 1(a) and 1(b). The DBA supports a broadband plasmonic resonance while the linear particle gratings provide frequency selective diffractive coupling through narrow-band photonic resonances. In order to strongly enhance the intensity of the plasmonic near-fields as well as to accurately control their frequency spectrum, we designed the nanoparticle chains to produce strong Fano-like photonic-coupling at the designed wavelengths (i.e., spectral overlap of photonic and plasmonic resonances). The particle sizes $a_{1,2}$ and particle diameters $d_{1,2}$ in the chains were optimized using three dimensional finite difference time domain (3D FDTD, Lumerical Solutions, Inc.) to produce the maximum near-field enhancement at the DBA central location when excited with a normally incident plane wave at 780 and 860 nm with the polarization direction indicated in Figs. 1(a) and 1(b). The Au nanoparticles, which are situated on a fused silica substrate, are 30 nm tall and designed using experimentally measured material dispersion [10]. The tips of triangles in the DBA have been rounded in the FDTD simulation to better describe the experimental situation, which is limited by the resolution of our nanofabrication process. The calculated electric near-field distributions of the grating-coupled plasmon resonances are visualized within the marked dashed regions of Figs. 1(a) and 1(b) for an excitation wavelength of 780 and 860 nm, respectively. Figure 1(c) shows the

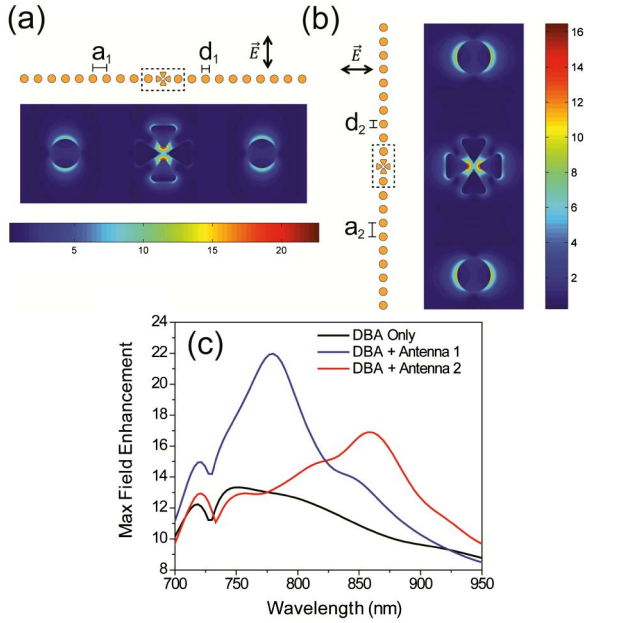

Fig. 1. (a) Antenna chain designed for near-field enhancement at 780 nm and near-field calculation of the electric field distribution in the dashed area at that wavelength. (b) Antenna chain designed for near field enhancement at 860 nm and near-field calculation of the electric field distribution in the dashed area at that wavelength. (c) Maximum near-field enhancement spectra in the DBA region for (black) DBA only, (blue) DBA and linear grating optimized for 780 nm [configuration 1(a)], and (red) DBA and linear grating optimized for 860 nm [configuration 1(b)].

calculated maximum near-field enhancement spectra of the antennas probed at the center of the DBA region for three different situations: (i) when an isolated DBA is excited (black), (ii) when the DBA is coupled to the chains designed to resonate at 780 nm (blue), and (iii) when the DBA is coupled to the chains designed to resonate at 860 nm (red). The chains are excited with the polarizations indicated by the arrows in the figure. It is well known that diffractive coupling between nanoparticles in linear gratings is maximized when both polarization and wave vector of the incident plane wave are perpendicular to the grating axis [11]. As can be observed in the near-field plots in Fig. 1, the single Au cylinders of the chains support dipolar resonances that are designed to spectrally overlap the DBA plasmon resonance, thus enhancing its nanoscale near-field intensity response in a tunable fashion [12]. Based on the described concept, we combine two linear chains of Au nanoparticles to produce a single multiwavelength nanoantenna device, shown in Fig. 2(a). The optimized lattice constants and particle diameters for the chain oriented at 0° are $a_1 = 540$ nm, $d_1 = 160$ nm, and for the chain oriented at 90° they are $a_2 = 600$ nm, $d_2 = 185$ nm. Figure 2(b) shows the DBA dimensions used, optimized for broadband near-field enhancement over the wavelengths of interest. An SEM of the fabricated antenna arrays on a fused silica substrate is shown in Fig. 2(c) and a closeup of the DBA is visible in Fig. 2(d), matching the dimensions used in the FDTD simulations. The Au nanoparticles were fabricated using an electron beam lithography (EBL) process, described previously in detail by Trevino *et al.* [13].

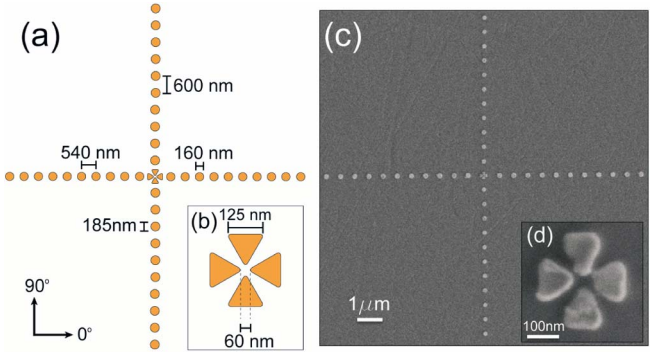

Fig. 2. (a) Optimized multiwavelength nanoantenna array geometry. (b) Double bow-tie antenna (DBA) at center of antenna array. (c) SEM micrograph of EBL fabricated gold nanoantenna array. (d) Close up SEM micrograph of DBA.

An array of periodically spaced multiwavelength nanoantennas was fabricated, covering an area 100 μm by 100 μm. The antennas were spaced sufficiently far apart (lattice constant = 16 μm) to avoid diffractive coupling of adjacent devices. In order to characterize the near-field resonant properties of the fabricated structure, we performed second harmonic excitation (SHE) spectroscopy. The technique has recently been shown to be an effective probe of photonic–plasmonic Fano-like coupling in arrays of metallic nanoparticles by Walsh and Dal Negro [14]. The generation of enhanced electromagnetic fields by excited plasmon resonances drives nonlinear harmonic generation from the metal nanoparticles [15]. Second harmonic generation (SHG) is a nonlinear process where a medium is excited by two photons at a fundamental frequency ω_0 and emits a single photon at twice that frequency $2\omega_0$.

The experimental setup utilized for the SHE characterization of the antenna arrays is sketched in the inset of Fig. 3(a). Laser pulses are generated by a tunable mode-locked Ti-Sapphire laser with 150 fs pulse duration and 82 MHz repetition rate. The excitation beam is focused on the array by a 20× microscope objective. A 700 nm long pass filter located before to the sample removes any SH signal produced by the optical components. The SHG is then collected in transmission with a 50×, 0.5NA objective. The signal is detected with a photon multiplier tube (PMT) coupled to a lock-in amplifier after passing through a monochromator. The excitation beam is removed with a 670 nm short pass filter prior to the monochromator. The sample is aligned with an imaging system consisting of a reflection microscope with a CCD camera, as shown. A removable mirror is placed in front of the camera to direct the SHG signal to the detector. The time-averaged excitation power is kept constant at 20 mW. The pump polarization is controlled by a half-wave liquid crystal variable retarder (Thorlabs LCC1111-B). In Fig. 3(a) we show the pump power dependence of the SHG signal detected at 380 nm for a representative array excited at 760 nm. The slope of the log–log plot demonstrates almost quadratic scaling ($m = 2.1$) of the signal with the incident intensity, consistent with the SHG process. Figure 3(c) shows the spatially averaged field enhancement in the DBA antenna feed gap calculated using 3D FDTD. To ensure the reproducibility of the simulated spectra, the area over which the

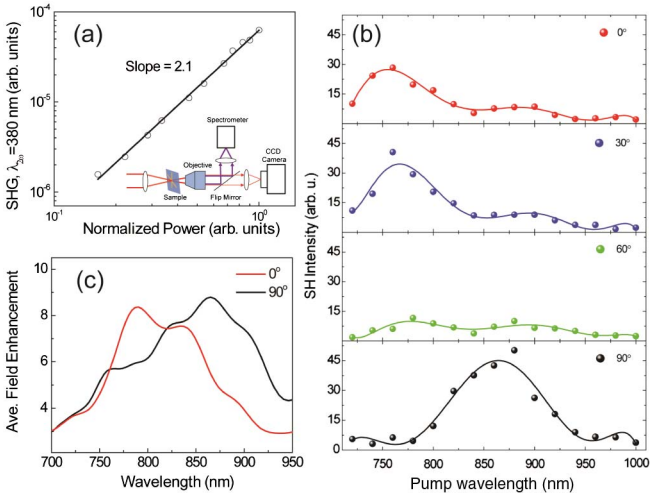

Fig. 3. (a) Pump ($\lambda_\omega = 760$ nm) power dependence of SH signal ($\lambda_{2\omega} = 380$ nm) from representative array. (Inset) Diagram of SH-E experimental setup. (b) Experimentally measured SH-E spectra of the antenna arrays as a function of the polarization angle as in the legend. (c) FDTD calculation of the spatially averaged near-field enhancement of the nanoantenna arrays for plane wave excitation with a polarization angle of 0° (red) and 90° (black).

field is spatially averaged was varied, resulting in no spectral changes, but only modifications in relative magnitude were observed. The antennas were excited with two orthogonal polarization states (0° and 90°). Notice that the resonance wavelength is controlled solely by the incident polarization. The experimentally measured SHE spectra of the antenna as a function of the polarization state are reported in Fig. 3(b). Data are normalized for the system response and for the pumping photon flux. Note that when the antenna is excited using a polarization angle of 0° (top panel), the SH-E spectrum peaks between 740 and 800 nm. A much weaker peak is detectable at longer wavelengths (850–950 nm). As the polarization direction is changed, the relative intensity of the two peaks becomes comparable. At a polarization angle of 90° (bottom panel), the first peak almost disappears, while the resonance on the right side of the spectrum is dominant. These results are consistent with the simulated average near-field enhancement and match the designed resonance wavelength for each polarization. We notice that in the experimental situation the arrays are excited using a focused laser beam, which has a range of k-vector components not present in the numerical calculations. Therefore, despite the fact that good agreement with FDTD calculations can only be considered qualitatively, our data clearly demonstrate polarization control over the spectral position of local field enhancement of radiatively coupled plasmon nanoantennas, as directly probed by their nonlinear SHG properties. These results could be further extended to longer wavelengths as recently demonstrated in the IR by Blanchard *et al.* [16].

In summary, we demonstrated a grating-assisted nanoantenna geometry that is polarization selective and allows for multiwavelength focusing into a subwavelength plasmon spot, in good agreement with full-vector FDTD simulations. We experimentally demonstrate the selective spectral response of such nanoantennas using SH-E spectroscopy. These structures can potentially open new paths for molecular linear and nonlinear spectroscopy, Raman spectroscopy, and near-field optical lithography with polarization controlled and spectral selectivity of hot spots.

The authors thank professor Federico Capasso and Mikhail Kats and Romain Blanchard at Harvard University for the insightful discussions. This work was supported by the NSF program "Multiparametric Optical Microbe Sensing with Engineered Photonic–Plasmonic Nanostructures" under Award CBET-1159552, and by the AFOSR program "Nanoscale Optical Emitters for High Density Information Processing using Photonic–Plasmonic Coupling in Coaxial Nanopillars" under Award FA9550-13-1-0011. NSRDEC PAO No. U13-268.

References

1. P. Biagioni, J.-S. Huang, and B. Hecht, Rep. Prog. Phys. **75**, 024402 (2012).
2. P. Bharadwaj, B. Deutsch, and L. Novotny, Adv. Opt. Photon. **1**, 438 (2009).
3. R. M. Bakker, H.-K. Yuan, Z. Liu, V. P. Drachev, A. V. Kildishev, V. M. Shalaev, R. H. Pedersen, S. Gresillon, and A. Boltasseva, Appl. Phys. Lett. **92**, 043101 (2008).
4. M. Sivis, M. Duwe, B. Abel, and C. Ropers, Nat. Phys. **9**, 304 (2013).
5. M. Navarro-Cia and S. A. Maier, ACS Nano **6**, 3537 (2012).
6. J. N. Anker, W. P. Hall, O. Lyandres, N. C. Shah, J. Zhao, and R. P. Van Duyne, Nat. Mater. **7**, 442 (2008).
7. R. Adato, A. A. Yanik, J. J. Amsden, D. L. Kaplan, F. G. Omenetto, M. K. Hong, S. Erramilli, and H. Altug, Proc. Natl. Acad. Sci. USA **106**, 19227 (2009).
8. H. A. Atwater and A. Polman, Nat. Mater. **9**, 205 (2010).
9. S. V. Boriskina and L. Dal Negro, Opt. Lett. **35**, 538 (2010).
10. P. B. Johnson and R. W. Christy, Phys. Rev. B **6**, 4370 (1972).
11. S. Zou and G. C. Schatz, J. Chem. Phys. **121**, 12606 (2004).
12. Z. Zhang, A. Weber-Bargioni, S. W. Wu, S. Dhuey, S. Cabrini, and P. J. Schuck, Nano Lett. **9**, 4505 (2009).
13. J. Trevino, H. Cao, and L. Dal Negro, Nano Lett. **11**, 2008 (2011).
14. G. F. Walsh and L. Dal Negro, Nano Lett. **13**, 3111 (2013).
15. C. Chen, A. De Castro, and Y. Shen, Phys. Rev. Lett. **46**, 145 (1981).
16. R. Blanchard, S. V. Boriskina, P. Genevet, M. A. Kats, J.-P. Tetienne, N. Yu, M. O. Scully, L. Dal Negro, and F. Capasso, Opt. Express **19**, 22113 (2011).